Characterizing Temperature and Strain Variations with Qubit Ensembles for Their Robust Coherence Protection

Guoqing Wang (□□□), Ariel Rebekah Barr, Hao Tang, Mo Chen (□□), Changhao Li (□□□), Haowei Xu, Andrew Stasiuk, Ju Li, and Paola Cappellaro

Phys. Rev. Lett. **131**, 043602 — Published 25 July 2023

DOI: 10.1103/PhysRevLett.131.043602

Characterizing temperature and strain variations with qubit ensembles for their robust coherence protection

Guoqing Wang (王国庆),[1,2,*] Ariel Rebekah Barr,[3,†] Hao Tang,[3,†] Mo Chen (陈墨),[1,4,5] Changhao Li (李长昊),[1,2] Haowei Xu,[2] Andrew Stasiuk,[1,2] Ju Li,[2,3,‡] and Paola Cappellaro[1,2,6,§]

[1] *Research Laboratory of Electronics, Massachusetts Institute of Technology, Cambridge, MA 02139, USA*
[2] *Department of Nuclear Science and Engineering, Massachusetts Institute of Technology, Cambridge, MA 02139, USA*
[3] *Department of Materials Science and Engineering, Massachusetts Institute of Technology, MA 02139, USA*
[4] *Thomas J. Watson, Sr., Laboratory of Applied Physics, California Institute of Technology, Pasadena, CA 91125, USA*
[5] *Institute for Quantum Information and Matter, California Institute of Technology, Pasadena, CA 91125, USA*
[6] *Department of Physics, Massachusetts Institute of Technology, Cambridge, MA 02139, USA*

Solid-state spin defects, especially nuclear spins with potentially achievable long coherence times, are compelling candidates for quantum memories and sensors. However, their current performances are still limited by dephasing due to variations of their intrinsic quadrupole and hyperfine interactions. We propose an *unbalanced echo* to overcome this challenge by using a second spin to refocus variations of these interactions, while preserving the quantum information stored in the nuclear spin free evolution. The unbalanced echo can be used to probe the temperature and strain distribution in materials. We develop first-principles methods to predict variations of these interaction and reveal their correlation over large temperature and strain ranges. Experiments performed in an ensemble of $\sim 10^{10}$ nuclear spins in diamond demonstrate a 20-fold dephasing time increase, limited by other noise sources. We further numerically show that our method can refocus even stronger noise variations than present in our experiments.

Solid-state spin defects are promising quantum platforms for sensing, communication and computing due to their favorable optical, spin, and charge properties [1]. For example, color centers in diamond have been used to sense rotation [2–5], magnetic and electric fields [6–8], temperature [9, 10] and pressure [11–14] with high resolution and precision [15]. Compatible with industry-standard fabrication process, donor spins in silicon [16] and defects in silicon carbide [17], also show potential in building quantum devices such as quantum sensors and quantum memories [18, 19]. More recently, nuclear spins in rare-earth doped crystals have attracted extensive interest to realize ensemble-based quantum memory and quantum network [20].

Scaling up the system size and improving control fidelity are crucial to realizing quantum advantage. One challenge is decoherence due to the system coupling to a noisy and inhomogeneous environment, as well as the lack of their in-depth characterization. In particular, while nuclear spins can serve as memories or sensors, electronic spins are usually needed for their control and readout via the hyperfine interaction, which then limits their coherence time. Although dynamical decoupling methods [21] in the spirit of spin echo [22] protect quantum system from these environmental noise sources, these sequences typically erase the stored quantum information, and break the sensor's sensitivity to low-frequency target fields. Potential solutions to such a dilemma include controlling the spin bath [23–25], encoding qubits in decoherence-free states [4, 5, 26, 27] or utilizing motional narrowing effects [28]. These techniques are however complex, as they require e.g., fast and high-fidelity control [25] or preparation of double-quantum states [4, 5, 26].

Here, we propose an *unbalanced echo* to protect quantum coherence against spatial or temporal variation of intrinsic interactions, which resembles a typical spin echo, but preserves quantum information acquired during the qubit's free evolution. We study the protection of the native ^{14}N nuclear spin near nitrogen-vacancy (NV) center in diamond and show that the optimal protection is achieved by flipping the NV electronic spin only once during the free evolution. Here we exploit hyperfine interaction, which is usually detrimental to the qubit coherence, to cancel out the noise effects. The flip time is set by the relative variation of the quadrupole Q of the nuclear spins and nuclear-NV hyperfine interaction A_{zz}. Experimentally, we achieve an order of magnitude improvement of the dephasing time of a $\sim 10^{10}$ spin ensemble. Theoretically, we develop a general first-principles approach to predict the strain and temperature dependence of intrinsic interactions. Our theoretical results indicate a strong correlation between interactions, dominated by the common phonon coupling, which enable robust coherence protection under extreme temperature or pressure conditions (e.g., 400× coherence improvement under a 25 K temperature variation). Moreover, our methods can be used to probe temperature and strain distributions in materials with nanoscale resolution. Our results pave the way to building highly sensitive sensors

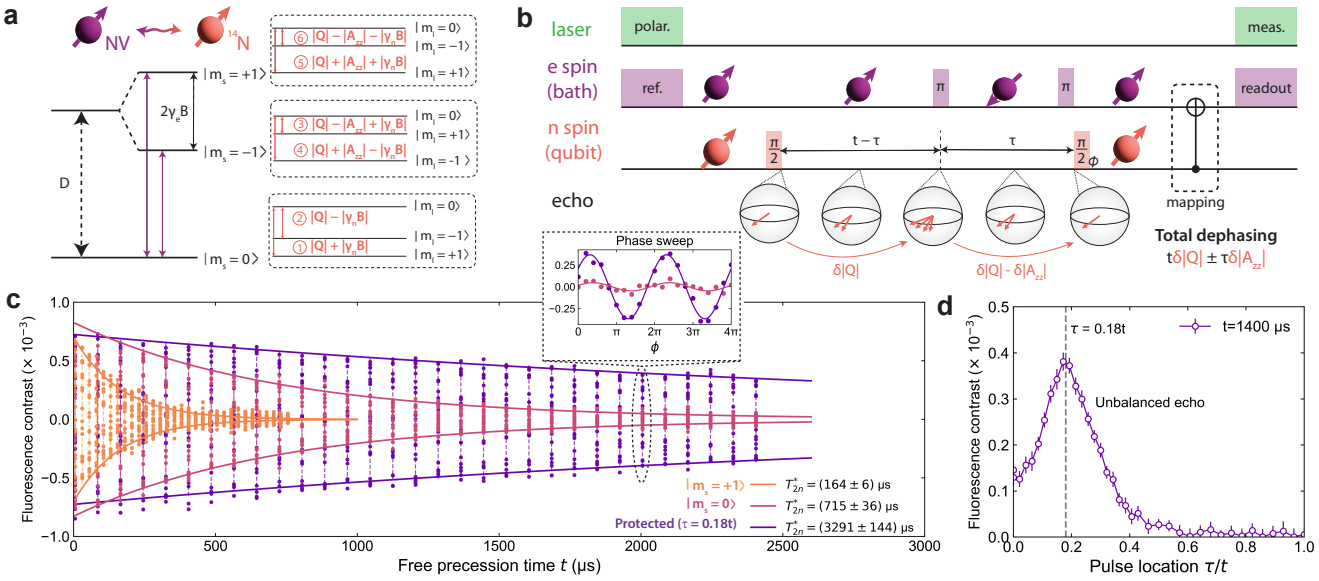

FIG. 1. **Coherence protection.** (a) Energy levels of NV ground state. (b) Coherence protection sequence. A laser pulse polarizes the NV to $|m_S = 0, m_I = +1\rangle$ state. The nuclear spin state $(|0\rangle + |\pm 1\rangle)/\sqrt{2}$ is prepared with a $\pi/2$ RF pulse. A microwave π pulse is applied to flip the NV electronic spin state from $|0\rangle$ to $|\pm 1\rangle$. A final π pulse transfer the NV state back to $|0\rangle$. The $\pi/2$ pulse applied to the nuclear spin associated with a conditional electronic spin π pulse performs a readout of the nuclear spin population. (c) Free evolution (Ramsey) measurements of unprotected and protected nuclear spin states $(|0\rangle + |-1\rangle)/\sqrt{2}$. At each time t, we sweep the phase of the last nuclear spin $\pi/2$ pulse to measure the coherence (inset). The amplitudes of the phase sweep measurements are fit to exponential decay. (d) Sweep of the pulse location τ/t with $t = 1400$ μs.

such as gyroscopes, thermometers and strain sensors, as well as long-lived and highly stable quantum memories using an ensemble of solid-state spins.

Unbalanced echo—The NV center in diamond has a spin-1 electronic ground state which can be optically polarized and read out in ambient conditions [29]. The nitrogen nuclide is also a spin-1 that can be polarized and read out via its hyperfine interaction with the electronic spin [30, 31]. The long coherence time of the nuclear spin enables applications such as gyroscopes [2–5] and quantum registers [32–34].

In a magnetic field B aligned with the NV center, its nuclear spin Hamiltonian includes quadrupole, hyperfine and Zeeman interaction terms,

$$H_n = QI_z^2 + m_S A_{zz} I_z + \gamma_n B I_z, \qquad (1)$$

where I_z is the spin-1 z operator, and we assume the NV electronic spin is in its eigenstate $|m_S\rangle$. As shown in Fig. 1(a), the single quantum (SQ) transitions between $|m_I = 0\rangle$ and $|m_I = \pm 1\rangle$ have six different frequencies $\omega_{1,2} = |Q| \pm |\gamma_n B|$, $\omega_{3,4} = |Q| \mp |A_{zz}| \pm |\gamma_n B|$ and $\omega_{5,6} = |Q| \pm |A_{zz}| \pm |\gamma_n B|$ corresponding to the electronic spin states $|m_S = 0\rangle$, $|m_S = -1\rangle$ and $|m_S = +1\rangle$, respectively.

In many scenarios, quantum information is stored in a superposition state undergoing free evolution $|\psi(t)\rangle = (|0\rangle + e^{i\varphi}|-1\rangle)/\sqrt{2}$, which accumulates a quantum phase $\varphi = \omega t$. When such a phase is used for sensing the qubit frequency ω, one measures the overlap between the final state and initial state yielding a Ramsey oscillation signal $S(t) = [1 + \cos(\omega t)]/2$. For an ensemble of qubits with a noisy environment, the measured signal is the average, $S(t) = [1 + \langle\cos(\omega t)\rangle]/2$, over the frequency distribution $\omega = \omega_0 + \delta\omega$. When $\delta\omega$ satisfies a zero-mean Lorenzian distribution with a half-width $\sigma = 1/T_2^*$, the signal has an exponential decay envelope $\langle\cos(\omega t)\rangle = \cos(\omega_0 t)e^{-t/T_2^*}$ characterizing the loss of quantum information. When the NV electronic spin is in $|m_S = 0\rangle$, the variation of the SQ transition frequency is $\delta\omega = \delta|Q| + \gamma_n \delta|B|$; when the NV is in $|m_S = \pm 1\rangle$, the variation is $\delta\omega = \delta|Q| \mp \delta|A_{zz}| + \gamma_n \delta|B|$. The variation of the magnetic field δB is usually minimized when designing the experimental setup, and the small gyromagnetic ratio $\gamma_n/\gamma_e \sim 10^{-4}$ introduces negligible coupling to the magnetic noise. Thus, the coherence time of the nuclear spin ensemble is largely limited by the variations in quadrupole and hyperfine interactions. The most common mechanisms include temperature and strain inhomogeneities introduced by laser heating and natural or applied strain in the material.

A powerful strategy for coherence protection is based on an echo sequence with a spin flip pulse applied in the middle of the free evolution such that the phases accumulated during the two halves of the total evolution cancel each other. However, this process also cancels the useful quantum phase information ω_0.

In contrast, we apply a spin flip to the NV elec-

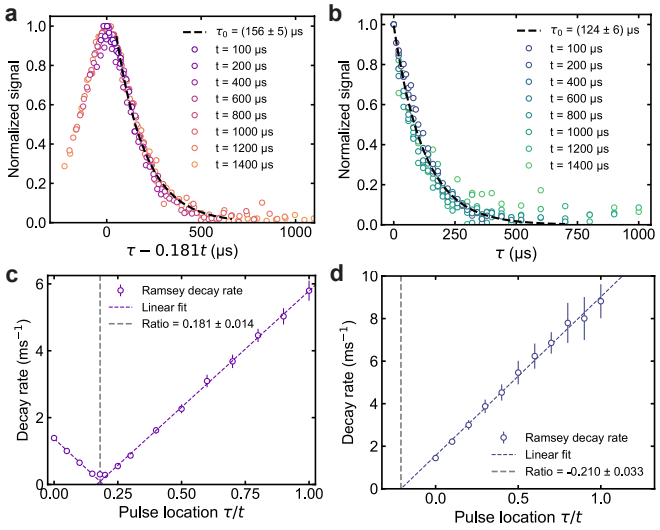

FIG. 2. **Inhomogeneity characterization.** (a,b) Sweep of pulse location τ/t under different free-precession times t. The electronic spin flip is between $|m_S=0\rangle$ and $|m_S=+1\rangle$. The nuclear spin in (a,b) is prepared in $(|0\rangle+|-1\rangle)/\sqrt{2}$, $(|0\rangle+|+1\rangle)/\sqrt{2}$, respectively. (c,d) Decay rate $1/T_{2n}^*$ as a function of τ/t for the same nuclear and electron spin states as in (a,b), respectively.

tronic spin. This is equivalent to effectively inverting the bath/environment state, as the NV mediates the effects of temperature and strain. The protocol works as long as the noise source affects both the quadrupole and hyperfine interactions regardless of the mechanism governing the relationship between the noise and the interactions. For example, in optically addressed solid-state spin ensembles, the laser heating introduces temperature variations δT. This correlates the variation of both interactions, which can be expressed as $\delta Q=\alpha_Q\delta T$, $\delta A_{zz}=\alpha_A\delta T$. To protect the target nuclear spin state $|\psi(0)\rangle$ prepared under the NV state $|m_S=0\rangle$, we flip the NV to $|m_S=+1\rangle$ at time $(t-\tau)$ in a free evolution duration t (Fig. 1(b)). The total phase accumulation of the target nuclear spin under δT is then $\varphi(\delta T)=\varphi_0+\delta\varphi$ with

$$\varphi_0=-tQ+\tau A_{zz}+\gamma_n Bt,\quad \delta\varphi=-(t\alpha_Q-\tau\alpha_A)\delta T. \quad (2)$$

When the pulse location τ/t is set to the ratio α_Q/α_A, the noise $\delta\varphi$ will be completely canceled while the static part φ_0 still remains sensitive to the magnetic field (or a rotation phase in gyroscopes), the mean quadrupole and hyperfine interactions, which are useful for various sensing applications.

Our protocol is experimentally demonstrated at room temperature in Fig. 1(c), where we compare the nuclear spin dephasing times with and without protection, showing one order of magnitude improvement in T_{2n}^*. We note that for both unprotected cases, the slightly longer dephasing time under $|m_S=0\rangle$ is caused by the vanishing hyperfine interaction contribution to the transition frequency. To visualize the refocusing effect, we fix the free-precession time and sweep the spin flip location in Fig. 1(d), where an *unbalanced echo* signal is observed at $\tau/t=0.18$.

Characterization of temperature and strain distribution— Our method can also probe the material-dependent ratio α_Q/α_A, and can be used to characterize the temperature distribution in the material by analyzing the shape and decay constant in the unbalanced echo and free evolution measurements. For instance, for a Lorentzian distribution of the temperature with half-width σ_T, the dephasing factor is

$$e^{-t/T_{2n}^*}=e^{-|t\alpha_Q\pm\tau\alpha_A|\sigma_T}=e^{-|\tau\pm\frac{\alpha_Q}{\alpha_A}t||\alpha_A|\sigma_T} \quad (3)$$

for nuclear spin states $(|0\rangle+|\pm1\rangle)/\sqrt{2}$, respectively [35]. In Figs. 2(a,b), we sweep the pulse location for different free-precession times. The overlap of the normalized data plotted as a function of shifted time validates the prediction in Eq. (3) and the exponential dependence on t indicates a Lorentzian distribution of the interaction constants variation. In Figs. 2(c,d), we measure the free-precession decay rate $1/T_{2n}^*$ as a function of the pulse location. The linear dependence on τ/t further validates the Lorentzian model and provides a better estimate of the ratio $\alpha_Q/\alpha_A\approx 0.181(0.014)$. This is consistent with reported values under a similar temperature range [36, 37] that measured $\delta Q/\delta T\approx 39(2)$ Hz/K and $\delta A_{zz}/\delta T\approx 204(11)$ Hz/K, yielding $\alpha_Q/\alpha_A\approx 0.19(0.014)$. The measured dephasing times without the unbalanced echo indicate temperature variation of $\sigma_T\sim 5$ K if we assume that the temperature variation is the dominant mechanism (see SM[38]).

When more than one independent noise source exists, (e.g., temperature, strain, electric fields, ...), variations in the interaction constants can be written as $\delta Q=\alpha_Q\delta T+\beta_Q\delta\epsilon+\cdots$, $\delta A_{zz}=\alpha_A\delta T+\beta_A\delta\epsilon+\cdots$, etc. Since temperature introduces a stress-free strain through thermal expansion, here ϵ represents additional strain induced by finite stresses. Our method can characterize the distribution of different sources given that the material-dependent constants $\alpha,\beta,\cdots$ can be separately measured by spin-resonance experiments and the ratios α_Q/α_A, $\beta_Q/\beta_A,\cdots$ are expected to be different. For example, when all noise sources satisfy a Lorentzian distribution with half-widths $\sigma_T,\sigma_\epsilon,\cdots$, the dephasing factor is $e^{-\chi}=e^{-|t\alpha_Q\pm\tau\alpha_A|\sigma_T-|t\beta_Q\pm\tau\beta_A|\sigma_\epsilon-\cdots}$. By experimentally measuring the qubit dephasing as a function of t,τ and comparing to the predicted formula, the distribution of the noise sources in the target material can be characterized including both the standard deviations $\sigma_T,\sigma_\epsilon,\cdots$ and the characteristic functions.

Refocusing strong noise variations— Weak noise will induce linear variations of the interaction, leading to a fixed ratio α_Q/α_A (or β_Q/β_A). The optimal coherence

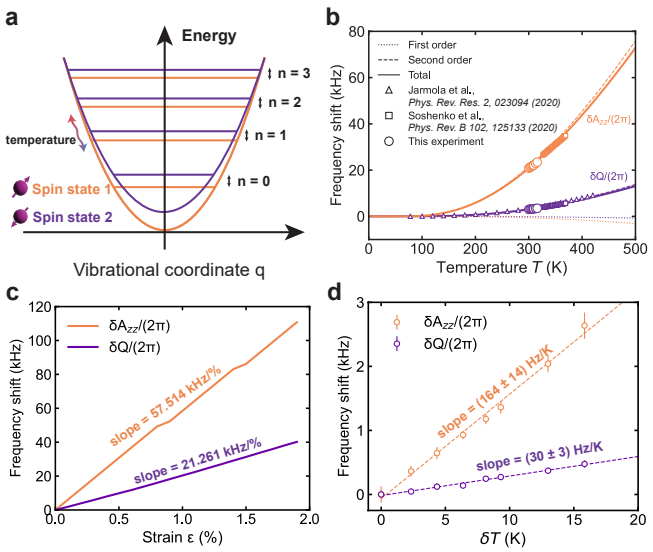

FIG. 3. **Theoretical model.** (a) Spin-phonon energy levels. (b) Calculated and measured shifts of δQ, δA_{zz} as a function of the temperature. Square and triangle data points are extracted from Soshenko *et al.* [36] and Jarmola *et al.* [37].(c) Calculated shifts of δQ, δA_{zz} as a function of the applied strain (compression). (d) Experimental measurements of frequency shifts as a function of temperature shifts.

protection is then achieved by setting the spin flip location τ/t to this fixed ratio, determined by the strongest noise. To extend our method to more general conditions, such as large temperature or strain variations, one needs to evaluate the correlation between quadrupole and hyperfine variations from a theoretical understanding of the underlining physical mechanism. The temperature influences the energy level through both (first-order) thermal expansion similar to pressure-induced strain [11] and (second-order) phonon distribution [37, 39], which changes the electron spin density and electric field gradient. The energy diagram forms a spin-dependent ladder separated by the phonon mode frequency as shown in Fig. 3(a). The spin transition frequency is then a weighted average of all the phonon states satisfying the Bose-Einstein distribution. Based on this analysis, we develop a predictive first-principles method to calculate the quadrupole and hyperfine variations, which is validated by the match with experiments in Fig. 3(b) and reveals the dominant role of phonons [40] [41] Our method can be extended to calculating other constants such as zero-phonon line, zero-field splitting in solid-state spin defects [40].

In Fig. 3(c), we calculate the hydrostatic strain dependence of both δQ, δA_{zz} and predict a relatively large linear range up to a ~ 26.6 GPa pressure (corresponding to $\epsilon = 2\%$), which has been validated in a recent experiment [42]. In high-pressure spectroscopy measurements, the strain inhomogeneity of the material could reach GPa levels resulting in limited spectral resolution [42, 43]. The predicted large linear range shows that our method can perfectly refocus at least a ~ 26 GPa pressure inhomogeneity, which paves the way to characterizing quantum materials in extreme conditions using quantum sensors. As strain (or electric field) has been used to tune the transitions in color centers in diamond [44, 45], as well as the hyperfine [46, 47] and quadrupole interactions [48] in the donor nuclear spins in silicon, our results make it possible to design high-fidelity strain control protocols for these applications.

Simulations in Fig. 4(a) show that the interaction variation ratios for both temperature and strain satisfy $\alpha_A/\alpha_Q, \beta_A/\beta_Q > 1$ (as required for $t/\tau > 1$ in unbalanced echo) over broad temperature and strain ranges, which demonstrates the broad applicability of our protection method. In addition, since temperature and strain have different ratios $\alpha_A/\alpha_Q \neq \beta_A/\beta_Q$, it is possible to characterize and distinguish the temperature and strain distributions in the material. Specifically, the ratio obtained from our unbalanced echo experiments matches the theoretical prediction from temperature variations (Fig. 4(a)), which indicates that our sample might be dominated by temperature variations. We note that other sources of noise, including local electric fields and charge dynamics in the host material, might contribute to the nuclear spin dephasing. It would be interesting to verify from first-principles and experiments the ratio $\delta Q/\delta A$ arising from the electric field, for example measuring nuclear spin dephasing under varying NV photoionization conditions [49, 50].

Using the first-principles results, we numerically study the spin dynamics over a large temperature inhomogeneity, to verify coherence protection beyond the linear regime. Indeed, a large temperature range results in a varying ratio between the two interactions, thus precluding to find an exact pulse location τ/t for the unbalanced echo. Still, using the optimal pulse location from Fig. 4(b) it is possible to achieve good protection, as shown in Fig. 4(c). For a 10 K temperature inhomogeneity, more than 122 ms dephasing time is achieved (assuming no other noise sources), showing a 1200-fold improvement.

Discussion— With variations in Q and A_{zz} refocused by the unbalanced echo, the achieved $T^*_{2n} = 3.5(0.4)$ ms (at $\tau/t = 0.2$) is ultimately limited by other magnetic noise sources such as field inhomogeneities and dipolar-coupled spin bath (see SM [38]). This dephasing time is comparable to what obtained with another strategy to cancel quadrupolar (and hyperfine) interaction variations, that is, using a double-quantum (DQ) superposition state $(|+1\rangle + |-1\rangle)/\sqrt{2}$ under the electronic spin states $|m_S = 0\rangle$ [4, 5, 26], giving a dephasing time $T^*_{2,DQ} = 3.6(0.3)$ ms [38]. In comparison to the DQ method which requires multi-tone driving control for state preparation and readout, our method only needs

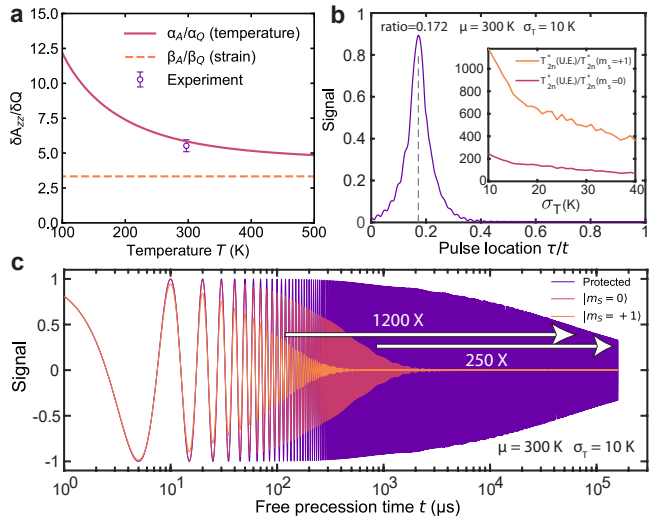

FIG. 4. **Refocusing large temperature inhomogeneities.** (a) Calculated ratios α_A/α_Q and β_A/β_Q as a function of temperature. The strain curve is the ratio between the two slopes in Fig. 3c. (b) Simulated unbalanced echo ($t = 2$ ms) for a qubit ensemble with a Lorentzian-shape temperature inhomogeneity. The nuclear spin state is $(|0\rangle+|-1\rangle)/\sqrt{2}$ and the electronic spin flips between $|m_S = 0\rangle$ and $|m_S = +1\rangle$. The coherence improvement factor versus inhomogeneity σ_T is shown in the inset. (c) Simulation of unprotected and protected ($\tau/t = 0.172$) Ramsey experiments (here we consider only temperature-induced dephasing and neglect other noise sources, including NV T_1.)

a simple SQ control which is more easily calibrated. Our method preserves the information of quadrupole and hyperfine interactions which are useful for quantum sensing [Eq. (2)]. Moreover, our method is applicable to other spin baths such as $S = 1/2$ electronic spins where the unbalanced echo condition for nuclear spin qubit is $t\delta Q + (t - 2\tau)\delta A = 0$, while the DQ method fails due to the always-on hyperfine. More broadly, in addition to protecting nuclear spin with $I > 1/2$ in platforms such as group V donors in silicon [19], rare earth ions in solids [20, 51, 52], and defects in hexagonal boron nitride [53, 54], the idea of canceling different interaction variations could be extended to other interactions existing in solid-state platforms such as electronic spin zero-field splitting and spin-orbit coupling.

Our method can completely refocus the spatial inhomogeneity dominated by a common source or several common sources with the same ratio between the variations of two interactions. When more than one effect with different ratios dominate, the optimal performance highly depends on those material constants $\alpha, \beta, \cdots$. However, one can still characterize the relative contributions of different sources and optimize the quantum device based on the obtained information, for example based on finite-element calculations of the thermomechanical fields $T(\mathbf{x})$, $\epsilon(\mathbf{x})$ where $\mathbf{x}$ is the spatial coordinate of the spin defect.

We note that the same method can also decouple time varying noise sources for both single and ensemble spins. In that scenario, it is convenient to keep the unbalanced echo time shorter than the noise correlation time and repeat the sequence multiple times, similar to the strategy adopted in multipulse dynamical decoupling [21].

A few promising directions include combining our method with dynamical decoupling to explore sensing of non-static quantities and concatenating our sequence with other coherence protection methods such as driving other bath spins to further push the coherence limit. As mentioned, our method finds an immediate application to improve nuclear spin gyroscopes [2–5, 55, 56] and quantum memory for quantum computation and sensing [32–34]. In addition, we envision further application in developing nanoscale sensors to probe temperature, strain and electric field distributions with high spectral resolution under extreme conditions such as high pressure; developing high-fidelity strain control with high spin in silicon donors; improving NMR frequency resolution [38].

This work were supported in part by DARPA DRINQS program (Cooperative Agreement No. D18AC00024), HRI-US, NSF DMR-1923976, NSF DMR-1923929 and NSF CMMI-1922206. A.R.B. acknowledges support from a National Science Foundation Graduate Research Fellowship under Grant No. DGE-174530. The calculations in this work were performed in part on the Texas Advanced Computing Center (TACC) and the MIT engaging cluster. G.W. thanks Thanh Nguyen for help in figure revision.

* gq_wang@mit.edu; These authors contributed equally.
† These authors contributed equally.
‡ liju@mit.edu
§ pcappell@mit.edu

[1] G. Wolfowicz, F. J. Heremans, C. P. Anderson, S. Kanai, H. Seo, A. Gali, G. Galli, and D. D. Awschalom, Quantum guidelines for solid-state spin defects, Nat. Rev. Mater. **6**, 906 (2021).
[2] A. Ajoy and P. Cappellaro, Stable three-axis nuclear-spin gyroscope in diamond, Phys. Rev. A **86**, 062104 (2012).
[3] J.-C. Jaskula, K. Saha, A. Ajoy, D. Twitchen, M. Markham, and P. Cappellaro, Cross-Sensor Feedback Stabilization of an Emulated Quantum Spin Gyroscope, Phys. Rev. Appl. **11**, 054010 (2019).
[4] A. Jarmola, S. Lourette, V. M. Acosta, A. G. Birdwell, P. Blümler, D. Budker, T. Ivanov, and V. S. Malinovsky, Demonstration of diamond nuclear spin gyroscope, Sci. Adv. **7**, eabl3840 (2021).
[5] V. V. Soshenko, S. V. Bolshedvorskii, O. Rubinas, V. N. Sorokin, A. N. Smolyaninov, V. V. Vorobyov, and A. V. Akimov, Nuclear spin gyroscope based on the nitrogen vacancy center in diamond, Phys. Rev. Lett. **126**, 197702 (2021).
[6] J. M. Taylor, P. Cappellaro, L. Childress, L. Jiang, D. Budker, P. R. Hemmer, A. Yacoby, R. Walsworth,

and M. D. Lukin, High-sensitivity diamond magnetometer with nanoscale resolution, Nat. Phys. **4**, 810 (2008).
[7] J. R. Maze, P. L. Stanwix, J. S. Hodges, S. Hong, J. M. Taylor, P. Cappellaro, L. Jiang, M. V. G. Dutt, E. Togan, A. S. Zibrov, A. Yacoby, R. L. Walsworth, and M. D. Lukin, Nanoscale magnetic sensing with an individual electronic spin in diamond, Nature **455**, 644 (2008).
[8] F. Dolde, H. Fedder, M. W. Doherty, T. Nöbauer, F. Rempp, G. Balasubramanian, T. Wolf, F. Reinhard, L. C. L. Hollenberg, F. Jelezko, and J. Wrachtrup, Electric-field sensing using single diamond spins, Nat. Phys. **7**, 459 (2011).
[9] G. Kucsko, P. C. Maurer, N. Y. Yao, M. Kubo, H. J. Noh, P. K. Lo, H. Park, and M. D. Lukin, Nanometre-scale thermometry in a living cell, Nature **500**, 54 (2013).
[10] J. Choi, H. Zhou, R. Landig, H.-Y. Wu, X. Yu, S. E. V. Stetina, G. Kucsko, S. E. Mango, D. J. Needleman, A. D. T. Samuel, P. C. Maurer, H. Park, and M. D. Lukin, Probing and manipulating embryogenesis via nanoscale thermometry and temperature control, Proc. Natl. Acad. Sci. U.S.A. **117**, 14636 (2020).
[11] M. W. Doherty, V. V. Struzhkin, D. A. Simpson, L. P. McGuinness, Y. Meng, A. Stacey, T. J. Karle, R. J. Hemley, N. B. Manson, L. C. L. Hollenberg, and S. Prawer, Electronic Properties and Metrology Applications of the Diamond NV - Center under Pressure, Phys. Rev. Lett. **112**, 047601 (2014).
[12] K. Y. Yip, K. O. Ho, K. Y. Yu, Y. Chen, W. Zhang, S. Kasahara, Y. Mizukami, T. Shibauchi, Y. Matsuda, S. K. Goh, and S. Yang, Measuring magnetic field texture in correlated electron systems under extreme conditions, Science **366**, 1355 (2019).
[13] M. Lesik, T. Plisson, L. Toraille, J. Renaud, F. Occelli, M. Schmidt, O. Salord, A. Delobbe, T. Debuisschert, L. Rondin, P. Loubeyre, and J.-F. Roch, Magnetic measurements on micrometer-sized samples under high pressure using designed nv centers, Science **366**, 1359 (2019).
[14] S. Hsieh, P. Bhattacharyya, C. Zu, T. Mittiga, T. J. Smart, F. Machado, B. Kobrin, T. O. Höhn, N. Z. Rui, M. Kamrani, S. Chatterjee, S. Choi, M. Zaletel, V. V. Struzhkin, J. E. Moore, V. I. Levitas, R. Jeanloz, and N. Y. Yao, Imaging stress and magnetism at high pressures using a nanoscale quantum sensor, Science **366**, 1349 (2019).
[15] C. L. Degen, F. Reinhard, and P. Cappellaro, Quantum sensing, Rev. Mod. Phys. **89**, 035002 (2017).
[16] J. J. L. Morton, A. M. Tyryshkin, R. M. Brown, S. Shankar, B. W. Lovett, A. Ardavan, T. Schenkel, E. E. Haller, J. W. Ager, and S. A. Lyon, Solid-state quantum memory using the 31P nuclear spin, Nature **455**, 1085 (2008).
[17] A. Bourassa, C. P. Anderson, K. C. Miao, M. Onizhuk, H. Ma, A. L. Crook, H. Abe, J. Ul-Hassan, T. Ohshima, N. T. Son, G. Galli, and D. D. Awschalom, Entanglement and control of single nuclear spins in isotopically engineered silicon carbide, Nat. Mater. **19**, 1319 (2020).
[18] F. A. Zwanenburg, A. S. Dzurak, A. Morello, M. Y. Simmons, L. C. L. Hollenberg, G. Klimeck, S. Rogge, S. N. Coppersmith, and M. A. Eriksson, Silicon quantum electronics, Rev. Mod. Phys. **85**, 961 (2013).
[19] A. Morello, J. J. Pla, P. Bertet, and D. N. Jamieson, Donor Spins in Silicon for Quantum Technologies, Adv. Quantum Technol. **3**, 2000005 (2020).
[20] A. Ruskuc, C.-J. Wu, J. Rochman, J. Choi, and A. Faraon, Nuclear spin-wave quantum register for a solid-state qubit, Nature **602**, 408 (2022).
[21] D. Suter and G. A. Álvarez, *Colloquium* : Protecting quantum information against environmental noise, Rev. Mod. Phys. **88**, 041001 (2016).
[22] E. L. Hahn, Spin Echoes, Phys. Rev. **80**, 580 (1950).
[23] E. Bauch, C. A. Hart, J. M. Schloss, M. J. Turner, J. F. Barry, P. Kehayias, S. Singh, and R. L. Walsworth, Ultralong Dephasing Times in Solid-State Spin Ensembles via Quantum Control, Phys. Rev. X **8**, 031025 (2018).
[24] H. S. Knowles, D. M. Kara, and M. Atatüre, Observing bulk diamond spin coherence in high-purity nanodiamonds, Nat. Mater. **13**, 21 (2014).
[25] M. Chen, W. K. C. Sun, K. Saha, J.-C. Jaskula, and P. Cappellaro, Protecting solid-state spins from a strongly coupled environment, New J. Phys. **20**, 063011 (2018).
[26] C. A. Hart, J. M. Schloss, M. J. Turner, P. J. Scheidegger, E. Bauch, and R. L. Walsworth, N - V –Diamond Magnetic Microscopy Using a Double Quantum 4-Ramsey Protocol, Phys. Rev. Appl. **15**, 044020 (2021).
[27] A. Reiserer, N. Kalb, M. S. Blok, K. J. M. van Bemmelen, T. H. Taminiau, R. Hanson, D. J. Twitchen, and M. Markham, Robust Quantum-Network Memory Using Decoherence-Protected Subspaces of Nuclear Spins, Phys. Rev. X **6**, 021040 (2016).
[28] P. C. Maurer, G. Kucsko, C. Latta, L. Jiang, N. Y. Yao, S. D. Bennett, F. Pastawski, D. Hunger, N. Chisholm, M. Markham, D. J. Twitchen, J. I. Cirac, and M. D. Lukin, Room-Temperature Quantum Bit Memory Exceeding One Second, Science **336**, 1283 (2012).
[29] M. W. Doherty, N. B. Manson, P. Delaney, F. Jelezko, J. Wrachtrup, and L. C. Hollenberg, The nitrogen-vacancy colour centre in diamond, Phys. Rep. **528**, 1 (2013).
[30] R. Fischer, A. Jarmola, P. Kehayias, and D. Budker, Optical polarization of nuclear ensembles in diamond, Phys. Rev. B **87**, 125207 (2013).
[31] T. Chakraborty, J. Zhang, and D. Suter, Polarizing the electronic and nuclear spin of the NV-center in diamond in arbitrary magnetic fields: Analysis of the optical pumping process, New J. Phys. **19**, 073030 (2017).
[32] A. Dréau, P. Spinicelli, J. R. Maze, J.-F. Roch, and V. Jacques, Single-Shot Readout of Multiple Nuclear Spin Qubits in Diamond under Ambient Conditions, Phys. Rev. Lett. **110**, 060502 (2013).
[33] P. Neumann, J. Beck, M. Steiner, F. Rempp, H. Fedder, P. R. Hemmer, J. Wrachtrup, and F. Jelezko, Single-Shot Readout of a Single Nuclear Spin, Science **329**, 542 (2010).
[34] G.-Q. Liu, J. Xing, W.-L. Ma, P. Wang, C.-H. Li, H. C. Po, Y.-R. Zhang, H. Fan, R.-B. Liu, and X.-Y. Pan, Single-shot readout of a nuclear spin weakly coupled to a nitrogen-vacancy center at room temperature, Phys. Rev. Lett. **118**, 150504 (2017).
[35] In general, the decay is related to the p.d.f. characteristic functions of the temperature and strain variations.
[36] V. V. Soshenko, V. V. Vorobyov, S. V. Bolshedvorskii, O. Rubinas, I. Cojocaru, B. Kudlatsky, A. I. Zeleneev, V. N. Sorokin, A. N. Smolyaninov, and A. V. Akimov, Temperature drift rate for nuclear terms of the NV-center ground-state Hamiltonian, Phys. Rev. B **102**, 125133 (2020).

[37] A. Jarmola, I. Fescenko, V. M. Acosta, M. W. Doherty, F. K. Fatemi, T. Ivanov, D. Budker, and V. S. Malinovsky, Robust optical readout and characterization of nuclear spin transitions in nitrogen-vacancy ensembles in diamond, Phys. Rev. Res. **2**, 023094 (2020).

[38] See Supplemental Material for details on the experimental measurements, analysis of coherence times and potential non-magnetic noise sources, simulations of large temperature variations, and an overview of potential applications of the unbalanced echo technique, which includes Refs. [2–5, 14, 19, 20, 23, 25, 33, 49–51, 54–68].

[39] M. W. Doherty, V. M. Acosta, A. Jarmola, M. S. J. Barson, N. B. Manson, D. Budker, and L. C. L. Hollenberg, Temperature shifts of the resonances of the NV - center in diamond, Phys. Rev. B **90**, 041201 (2014).

[40] H. Tang, A. R. Barr, G. Wang, P. Cappellaro, and J. Li, First-Principles Calculation of the Temperature-Dependent Transition Energies in Spin Defects, J. Phys. Chem. Lett. **14**, 3266 (2023).

[41] Since the offset of the frequency is a free parameter, experimental results are shifted to match the simulation results.

[42] Y.-X. Shang, F. Hong, J.-H. Dai, Y.-N. Lu, H. Yu, Y.-H. Yu, X.-H. Yu, X.-Y. Pan, and G.-Q. Liu, High-pressure nmr enabled by diamond nitrogen-vacancy centers (2022), arXiv:2203.10511 [quant-ph].

[43] Z. Wang, C. McPherson, R. Kadado, N. Brandt, S. Edwards, W. Casey, and N. Curro, Ac Sensing Using Nitrogen-Vacancy Centers in a Diamond Anvil Cell up to 6 GPa, Phys. Rev. Appl. **16**, 054014 (2021).

[44] P. Udvarhelyi, V. O. Shkolnikov, A. Gali, G. Burkard, and A. Pályi, Spin-strain interaction in nitrogen-vacancy centers in diamond, Phys. Rev. B **98**, 075201 (2018).

[45] S. Meesala, Y.-I. Sohn, B. Pingault, L. Shao, H. A. Atikian, J. Holzgrafe, M. Gündoğan, C. Stavrakas, A. Sipahigil, C. Chia, R. Evans, M. J. Burek, M. Zhang, L. Wu, J. L. Pacheco, J. Abraham, E. Bielejec, M. D. Lukin, M. Atatüre, and M. Lončar, Strain engineering of the silicon-vacancy center in diamond, Phys. Rev. B **97**, 205444 (2018).

[46] J. Mansir, P. Conti, Z. Zeng, J. J. Pla, P. Bertet, M. W. Swift, C. G. Van de Walle, M. L. W. Thewalt, B. Sklenard, Y. M. Niquet, and J. J. L. Morton, Linear Hyperfine Tuning of Donor Spins in Silicon Using Hydrostatic Strain, Phys. Rev. Lett. **120**, 167701 (2018).

[47] G. Wolfowicz, M. Urdampilleta, M. L. W. Thewalt, H. Riemann, N. V. Abrosimov, P. Becker, H.-J. Pohl, and J. J. L. Morton, Conditional Control of Donor Nuclear Spins in Silicon Using Stark Shifts, Phys. Rev. Lett. **113**, 157601 (2014).

[48] D. P. Franke, F. M. Hrubesch, M. Künzl, H.-W. Becker, K. M. Itoh, M. Stutzmann, F. Hoehne, L. Dreher, and M. S. Brandt, Interaction of Strain and Nuclear Spins in Silicon: Quadrupolar Effects on Ionized Donors, Phys. Rev. Lett. **115**, 057601 (2015).

[49] G. Wang, C. Li, H. Tang, B. Li, F. Madonini, F. F. Alsallom, W. K. C. Sun, P. Peng, F. Villa, J. Li, and P. Cappellaro, Manipulating solid-state spin concentration through charge transport (2023), arXiv:2302.12742 [cond-mat, physics:quant-ph].

[50] G. Wang, F. Madonini, B. Li, C. Li, J. Xiang, F. Villa, and P. Cappellaro, Fast wide-field quantum sensor based on solid-state spins integrated with a SPAD array (2023), arXiv:2302.12743 [physics, physics:quant-ph].

[51] D. D. Awschalom, R. Hanson, J. Wrachtrup, and B. B. Zhou, Quantum technologies with optically interfaced solid-state spins, Nat. Photon. **12**, 516 (2018).

[52] I. Nakamura, T. Yoshihiro, H. Inagawa, S. Fujiyoshi, and M. Matsushita, Spectroscopy of single Pr3+ ion in LaF3 crystal at 1.5 K, Sci. Rep. **4**, 7364 (2015).

[53] A. Gottscholl, M. Diez, V. Soltamov, C. Kasper, A. Sperlich, M. Kianinia, C. Bradac, I. Aharonovich, and V. Dyakonov, Room temperature coherent control of spin defects in hexagonal boron nitride, Sci. Adv. **7**, eabf3630 (2021).

[54] A. J. Healey, S. C. Scholten, T. Yang, J. A. Scott, G. J. Abrahams, I. O. Robertson, X. F. Hou, Y. F. Guo, S. Rahman, Y. Lu, M. Kianinia, I. Aharonovich, and J.-P. Tetienne, Quantum microscopy with van der Waals heterostructures, Nat. Phys. **19**, 87 (2023).

[55] M. P. Ledbetter, K. Jensen, R. Fischer, A. Jarmola, and D. Budker, Gyroscopes based on nitrogen-vacancy centers in diamond, Phys. Rev. A **86**, 052116 (2012).

[56] D. Maclaurin, M. W. Doherty, L. C. L. Hollenberg, and A. M. Martin, Measurable quantum geometric phase from a rotating single spin, Phys. Rev. Lett. **108**, 240403 (2012).

[57] M. Pfender, N. Aslam, H. Sumiya, S. Onoda, P. Neumann, J. Isoya, C. A. Meriles, and J. Wrachtrup, Nonvolatile nuclear spin memory enables sensor-unlimited nanoscale spectroscopy of small spin clusters, Nat. Commun. **8**, 834 (2017).

[58] T. Unden, P. Balasubramanian, D. Louzon, Y. Vinkler, M. B. Plenio, M. Markham, D. Twitchen, A. Stacey, I. Lovchinsky, A. O. Sushkov, M. D. Lukin, A. Retzker, B. Naydenov, L. P. McGuinness, and F. Jelezko, Quantum Metrology Enhanced by Repetitive Quantum Error Correction, Phys. Rev. Lett. **116**, 230502 (2016).

[59] B. J. Shields, Q. P. Unterreithmeier, N. P. de Leon, H. Park, and M. D. Lukin, Efficient readout of a single spin state in diamond via spin-to-charge conversion, Phys. Rev. Lett. **114**, 136402 (2015).

[60] Y.-X. Shang, F. Hong, J.-H. Dai, Y.-N. Lu, H. Yu, Y.-H. Yu, X.-H. Yu, X.-Y. Pan, and G.-Q. Liu, High-Pressure NMR Enabled by Diamond Nitrogen-Vacancy Centers (2022), arXiv:2203.10511 [quant-ph].

[61] J.-H. Dai, Y.-X. Shang, Y.-H. Yu, Y. Xu, H. Yu, F. Hong, X.-H. Yu, X.-Y. Pan, and G.-Q. Liu, Optically Detected Magnetic Resonance of Diamond Nitrogen-Vacancy Centers under Megabar Pressures, Chin. Phys. Lett. **39**, 117601 (2022).

[62] H. Chen, N. F. Opondo, B. Jiang, E. R. MacQuarrie, R. S. Daveau, S. A. Bhave, and G. D. Fuchs, Engineering Electron–Phonon Coupling of Quantum Defects to a Semiconfocal Acoustic Resonator, Nano Lett. **19**, 7021 (2019).

[63] G.-Q. Liu, X. Feng, N. Wang, Q. Li, and R.-B. Liu, Coherent quantum control of nitrogen-vacancy center spins near 1000 kelvin, Nat. Commun. **10**, 1344 (2019).

[64] E. Bauch, S. Singh, J. Lee, C. A. Hart, J. M. Schloss, M. J. Turner, J. F. Barry, L. M. Pham, N. Bar-Gill, S. F. Yelin, and R. L. Walsworth, Decoherence of ensembles of nitrogen-vacancy centers in diamond, Phys. Rev. B **102**, 134210 (2020).

[65] Z. Wang, J. Zhang, X. Feng, and L. Xing, Microwave Heating Effect on Diamond Samples of Nitrogen-Vacancy Centers, ACS Omega **7**, 31538 (2022).

[66] C. Szczuka, M. Drake, and J. A. Reimer, Effects of laser-

induced heating on nitrogen-vacancy centers and single-nitrogen defects in diamond, J. Phys. D: Appl. Phys. **50**, 395307 (2017).

[67] D. Duan, V. K. Kavatamane, S. R. Arumugam, G. Rahane, G.-X. Du, Y.-K. Tzeng, H.-C. Chang, and G. Balasubramanian, Laser-induced heating in a high-density ensemble of nitrogen-vacancy centers in diamond and its effects on quantum sensing, Opt. Lett. **44**, 2851 (2019).

[68] Z. Bai, Z. Zhang, K. Wang, J. Gao, Z. Zhang, X. Yang, Y. Wang, Z. Lu, and R. P. Mildren, Comprehensive Thermal Analysis of Diamond in a High-Power Raman Cavity Based on FVM-FEM Coupled Method, Nanomaterials **11**, 1572 (2021).